UC Berkeley
UC Berkeley Previously Published Works

Title

DIFFUSION-CONTROLLED EVAPORATING PERFECTLY WETTING MENISCUS IN A CHANNEL

Permalink

Journal

ISSN

Authors

Njante, Jean-Pierre
Morris, SJS

Publication Date

DOI

Peer reviewed

Diffusion-controlled evaporating perfectly wetting meniscus in a channel

Jean-Pierre Njante* and S.J.S. Morris

Department of Mechanical Engineering

University of California

Berkeley, California 94720

July 28, 2012

1 Though diffusion-controlled evaporation from capillaries has been studied
2 since the work of Stefan, except for the work of Derjaguin et al. (1965), the
3 interface is treated as a plane surface having known contact angle of $90°$.
4 Here, by contrast, the interface location is determined as part of the solution
5 of a free boundary problem coupling hydrodynamic and diffusion fields. We
6 make the following simplifying assumptions. (a) Liquid and vapour at the
7 interface are in local thermodynamic equilibrium; as a result, evaporation is
8 limited by diffusion of the vapour molecules in the gas. (b) The system is

*jpnjante@berkeley.edu

1

effectively isothermal; though evaporation induces liquid temperature differences, they are kinetically negligible. Given (a) and (b), the vapour partial pressure is related to the liquid pressure by the Kelvin equation. Though the hydrostatic contact angle is zero, the stationary evaporating meniscus exhibits an apparent contact angle; Θ is determined chiefly by a capillary number $Ca = \mu_\ell V_s / \gamma$ based on surface tension γ, liquid viscosity μ_ℓ, and a velocity scale V_s set by evaporation. Though microphysics must be included in the free boundary problem in order to resolve a hydrodynamic singularity at the contact line, Θ is insensitive to the microphysical details.

1   Introduction

Poulard et al. (2005) have studied experimentally and theoretically the evaporation of a droplet of chemically pure liquid from a perfectly wetted substrate into a mixture of vapour phase with an inert component. For their experimental conditions, evaporation is controlled by steady diffusion within the gas mixture. According to the well-known solution for that diffusion problem, evaporation is concentrated near the apparent contact line. Conservation of mass requires liquid flow towards the contact region, and the pressure differences induced to drive this liquid flow also distort the liquid-gas interface. As a result, the perfectly wetting evaporating system exhibits an apparent contact angle: Θ is a property of the small-scale flow induced by the evaporation, and vanishes (for a perfectly-wetting system) at equilibrium. The authors show that the time evolution of the droplet planform radius can be understood, at least qualitatively, by assuming the droplet to

2

be a spherical cap, and combining a mass balance including evaporative losses with a constitutive equation relating Θ to evaporation rate and to contact line velocity. This constitutive equation was written down using heuristic reasoning.

As a first step towards deriving a quantitative expression for the apparent contact angle in that geometry, here we pose and solve completely the free boundary problem describing the evaporating meniscus of a perfectly wetting liquid in a long narrow channel. This geometry offers two advantages over that of the droplet. The meniscus can be kept stationary in an experiment and, provided the capillary number based on the evaporatively–induced liquid flow is small, the mathematical problem is one–dimensional. Owing to a separation of lengthscales, its numerical solution is not trivial, however. In order for vapour diffusion from the meniscus to the channel mouth to be approximately one–dimensional, the channel must be long compared with the wall spacing. As a result, the thin wetting films on each wall are also long. As shown by Derjaguin et al.(1965), in very narrow channels, mass transport by liquid flow along these films can be comparable to the axial mass flow by diffusion along the gas column. Our numerical scheme must resolve those large–scale axial features, in addition to the small–scale axial flow occurring within the apparent contact region where the apparent contact angle is formed. Using these numerical solutions, we show that the meniscus exhibits an apparent contact angle Θ varying as the cube root of the capillary number based on evaporation rate. (Of course we also predict the evaporation rate as a function of experimentally–controllable parameters.)

2 Boundary Value Problem

Figure 1 shows the geometry of interest: an evaporating meniscus of a completely wetting pure liquid with uniform surface tension γ is formed in the gap between two horizontal flat plates of gap thickness $2a$. The plates are initially at common temperature T_w with the surroundings. The pure liquid evaporates into a binary mixture of its own vapour and an inert component. Evaporation occurs because the vapour partial pressure decreases from its saturation value p_{sat} at the bulk meniscus to ϕp_{sat} at the channel exit; here, ϕ is the relative humidity in the distant gas and p_{sat} the saturation vapour pressure at the uniform temperature T_w of the channel walls. Evaporation draws liquid into the contact region; near the wetted walls, the resulting pressure differences distort the phase interface, creating an apparent contact angle, Θ. We define the origin O at the point where the visible meniscus appears to intersect the lower wall, and define L as the distance from O to the channel exit; to keep the interface fixed relative to the wall, liquid is continuously fed into the channel at the same rate $2\dot{m}$ as it is being evaporated.

Because the liquid is completely wetting, the visible meniscus is preceded by a thin wetting film; we assume that within this thin film, disjoining pressure Π is related to film thickness h_* by $\Pi = A/h_*^3$, where A is the dispersion constant. Together A and γ define a length scale $(A/\gamma)^{1/2}$; this length scale is of molecular dimensions. We assume that the channel gap thickness $2a$ is large compared with the molecular scale; $1 \gg [A/(a^2\gamma)]^{1/2}$. Owing to this separation of scales, the extended meniscus has an inner–and–outer structure: for $\phi = 1$, the system is in hydrostatic equilibrium; for this case, Renk et al (1978) showed that the outer visible meniscus is a semicircle of radius

4

a; the inner solution consists of a non–uniform wetting film in which the capillary and disjoining pressures are comparable in magnitude. Far from the apparent contact line, defined by the intersection of the semicircle with the channel walls, the thickness of the wetting film approaches the uniform value $(aA/\gamma)^{1/3}$; this thickness is, of course, small compared with a. In this paper, we analyse the effect of evaporation on that hydrostatic picture.

To analyse the evaporating meniscus, we use the separation of scales described above. The inner region now consisting of the quasi–parallel liquid film, and the corresponding portion of the gas column. Within this region, the lubrication approximation holds within the film and, across the gas column, the partial pressure is uniform. Owing to these two conditions, the unknowns depend only on distance along the wall, and the mass transport within the inner region is determined by problem (1) containing only ordinary differential equations. For the gas, the outer region is bounded by the visible circular arc meniscus, and the chord joining the points where that meniscus intersects the channel walls. Within this region, the vapour partial pressure p_v^* satisfies the steady diffusion equation subject to the boundary condition that on the gas–liquid interface, $p_v^* = p_{sat}$, together with the boundary condition that on the chord, p_v^* matches to the solution of the inner problem.

We assume that the capillary number $\nu_\ell \dot{m}/a\gamma$ based on liquid kinetic viscosity ν_ℓ and (half) the evaporation-rate $\dot{m}$ is small compared with unity. This condition ensures that on the length scale a, the interface remains a circular arc even in the presence of evaporation. Within the contact region, however, the pressure differences required to drive liquid towards the region of maximum evaporation become sufficiently large to distort the phase interface.

106 Within this region, the unknowns $p_v^*(x_*)$, $p_\ell^*(x_*)$, $h_*(x_*)$, and the constant $\dot{m}$

107 are determined by the following free boundary value problem,

$$\dot{m} = \frac{h_*^3}{3\nu_\ell}\frac{dp_\ell^*}{dx_*} + \frac{aD_v}{R_vT_w}\frac{dp_v^*}{dx_*}, \tag{1a}$$

$$p - p_\ell^* = \gamma\frac{d^2h_*}{dx_*^2} + \frac{A}{h_*^3}, \tag{1b}$$

$$p_v^* = p_{sat} + \frac{\rho_{sat}}{\rho_\ell}(p_\ell^* - p_b); \tag{1c}$$

$$p_v^*(-L) = \phi p_{sat}, \qquad p_v^*(x_* \to a) \to p_{sat}, \tag{1d,e}$$

$$h_*(-L) = \left(\frac{A}{p - p_\ell^*}\right)^{\frac{1}{3}}, \qquad \frac{d^2h_*}{dx_*^2}(x_* \to a) \to \frac{1}{a} \tag{1f,g}$$

108 where ρ_ℓ is the liquid density, p_b the bulk liquid pressure, p the total pressure

109 in the gas, R_v the specific gas constant, D_v the binary diffusion coefficient,

110 and ρ_{sat} the saturation vapour density at T_w. We now interpret (1).

111 Equation (1a) is a statement of mass balance across a cross-section of the

112 channel. It expresses the mass flow rate $\dot{m}$ due to evaporation in the lower

113 half of the channel as the sum of the mass flow rates occurring within the

114 liquid and gas phases. On the right hand side, the first term describes the

115 mass flow due to a Poiseuille flow within the thin quasi-parallel liquid film;

116 the second term describes the mass flow by axial diffusion of vapour through

117 the gas column, and is merely the simplified form of Fick's first law,

$$\dot{m}_x = -\frac{aD_v}{R_vT_w}\frac{dp_v^*}{dx^*}, \qquad J^* = \frac{d\dot{m}_x}{dx^*} \tag{2a,b}$$

118 Equation (2) neglects the motion induced within the gas mixture; it is a

119 good approximation when the saturation vapour pressure is small compared

6

with the total pressure in the gas. The full form of that equation, including induced motion in the gas, is given as equation (28a) in appendix A.3. The mass balance equation (1a) also neglects Marangoni flows; this is a good approximation if the liquid is chemically pure, and temperature differences along the liquid–gas interface are negligibly small.

Equation (1b) is a statement of force balance normal to the interface. It states that the pressure force on an interfacial element balances the resultant force due to capillarity and disjoining pressure. On the right hand side, the first term gives the equation of capillarity for a slowly tapered film, whose slope is significantly small compared with unity; the second term describes the disjoining pressure for a uniform film. Here, the adsorption forces are restricted to the London-van der Waals dispersion forces. Even though Truong and Wayner (1993) and Levinson et al (1993, figure 3) showed that the inverse cube dependence for the disjoining pressure is appropriate only for film thicknesses less than $20nm$, we use it here as the effects of disjoining pressure become insignificant for film thicknesses greater than that anyway.

Equation (1c) is a simplification of the Hertz-Knudsen equation, see the discussion in appendix A.1. It states that liquid and vapour at the interface are in local thermodynamic equilibrium; as a result, evaporation is controlled by stationary diffusion of the vapour molecules in the gas. Though evaporation induces liquid temperature differences, we have assumed that they are kinetically negligible; this approximation is justified in Appendix A.2. In the model of the Stefan diffusion tube described by Bird et al (2006, §18.2), the kinetic equation (1c) is simplified by assuming that liquid pressure differences are negligibly small, even within the contact region where evaporation

7

is strongest. By accounting for liquid pressure differences, equation (1c) couples the dynamical processes in the liquid to those in the gas phase.

Boundary conditions (1e,g) are obtained by matching the outer limit of the inner solution to the inner limit of the outer solution. Specifically, boundary condition (1g) ensures that the interface curvature at the outer edge of the inner region matches smoothly to the uniform curvature of the outer circular arc meniscus; the other boundary condition (1e) is a matching condition on the vapour partial pressure. The vapour pressure at the outer edge of the inner region is equal to the saturation vapour pressure because for small capillary number, changes in liquid pressure along the outer meniscus are negligibly small. Therefore $p_\ell^* = p_b$ to a first approximation, and it follows from equation (1c) that $p_v^* = p_{sat}$ along the outer circular arc meniscus.

Because capillary pressure is negligible within the long tapered wetting film, boundary condition (1f) on the film thickness at the channel mouth is obtained by setting surface tension $\gamma = 0$ in equation (1b). This is the thin film solution described by Derjaguin et al (1965). The other boundary condition (1d) fixes the vapour pressure at the channel mouth. Unlike the outer boundary conditions (1e,g), we did not use the asymptotic forms for the film thickness and liquid pressure along the long tapered film because that asymptotic solution contains the mass flow $\dot{m}$, which is not known a priori. According to equation (1g), the film thickness grows parabolically with distance as $x_* \to a$; the effects of disjoining pressure are therefore negligible at the outer edge of the inner region. Consequently, the outer limit of the stress equation (1b) requires that we chose the constant $p_b = p - \gamma/a$.

We non-dimensionalize (1) by letting,

8

$$\Theta_s = \left(\frac{A}{\gamma a^2}\right)^{\frac{1}{6}}, \qquad h_s = a\Theta_s^2, \qquad x_s = a\Theta_s \qquad \text{(3a-c)}$$

where h_s and x_s are the characteristic dimensions of the contact region for hydrostatic state (Renk et al. 1978, equations 2, 10, 21). In the numerical analysis described in §3, we start with the hydrostatic solution and then use continuation to obtain solutions for $\phi < 1$; the film thickness scale h_s and the axial scale x_s are convenient choices for that numerical analysis.

We introduce dimensionless variables (without asterisks) by

$$p_\ell = \frac{a}{\gamma}(p_\ell^* - p_b), \qquad x = \frac{x_*}{x_s}, \qquad h = \frac{h_*}{h_s}. \qquad \text{(4a-c)}$$

To non-dimensionalize (1), we first eliminate the vapour partial pressure in favour of the liquid pressure using equation (1c); then substituting (4) into the resulting problem (1), we find that the unknowns h and p_ℓ satisfy the following dimensionless boundary value problem: for $-\chi/\Theta_s \leq x < \infty$,

$$\frac{d}{dx}\left[\left(\frac{h^3}{3\beta} + 1\right)\frac{dp_\ell}{dx}\right] = 0, \qquad \text{(5a)}$$

$$1 - p_\ell = \frac{d^2h}{dx^2} + \frac{1}{h^3}; \qquad \text{(5b)}$$

$$p_\ell(-\chi/\Theta_s) = -\alpha, \qquad p_\ell(x \to \infty) \to 0, \qquad \text{(5c,d)}$$

$$h(-\chi/\Theta_s) = \left(\frac{1}{1+\alpha}\right)^{\frac{1}{3}}, \quad h(x \to \infty) \to \frac{x^2}{2} \qquad \text{(5e,f)}$$

We have differentiated equation (1a) once so as to eliminate the integration constant $\dot{m}$. Boundary conditions (5d,f) are applied at infinity because the

9

slope unit $\Theta_s << 1$ owing to the separation of length scales described at the beginning of this section. However, boundary conditions (5c,e) are not applied at minus infinity because for $x < 0$, the solution continues to depend upon χ through the length of the gas column. Matching condition (1g) on the interface curvature far from the apparent contact line has been integrated and replaced with its asymptotic form (5f). Because the independent variable now appears explicitly in that boundary condition, the problem is no longer autonomous; as a result, the origin is fixed at the apparent contact line and can no longer be arbitrarily chosen. Four independent parameters appear in the dimensionless boundary value problem, namely; α, β, χ, and Θ_s.

$$\alpha = \frac{a\rho_\ell}{\gamma\rho_{sat}}p_{sat}(1 - \phi), \qquad \beta = \frac{\nu_\ell \rho_{sat}\gamma D_v}{\rho_\ell R_v T_w A}, \qquad \chi = \frac{L}{a} \qquad \text{(6a-c)}$$

According to equations $(1c, d, e)$, the liquid pressure decreases from p_b at the bulk meniscus to $p_b - \rho_\ell p_{sat}(1 - \phi)/\rho_{sat}$ at the channel mouth; α is the ratio of the pressure-difference $\rho_\ell p_{sat}(1 - \phi)/\rho_{sat}$ driving the resulting flow to the pressure-difference γ/a across the bulk meniscus. For fixed α and position x, the parameter β controls the fraction of the total mass flow transported by axial diffusion in the gas. The parameter χ is the channel's aspect ratio.

For use in subsequent analysis, we define

$$f = \frac{\dot{m}}{\dot{m}_s} \qquad \text{where} \qquad \dot{m}_s = \frac{aD_v p_{sat}}{R_v T_w L}(1 - \phi) \qquad \text{(7a,b)}$$

According to the simplified form of Fick's law, $\dot{m}_s$ is the diffusive transport caused by a gradient $(1 - \phi)p_{sat}/L$ of vapour concentration. The integration constant f is the ratio of the total evaporation from the capillary to $\dot{m}_s$.

10

Table 1 shows representative values for the parameters in the theory. We have used $A = 10^{-21}J$ for the dispersion constant, $a = 10\mu m$ for capillary radius, and $\phi = 0.3$ for the relative humidity in the distant gas. All material properties are evaluated at the uniform wall temperature $T_w = 298K$. The slope unit Θ_s is small as expected whereas α is generally large, except when the system is near hydrostatic equilibrium. In general, $0.01 < \beta < 1$.

3 Numerical Method

The governing equations (5) are numerically solved using the NAG routine D02TKF, which uses the collocation method to approximate the solution at certain specified locations within the problem domain; solution values anywhere else within the problem domain are obtained using polynomial interpolation. The routine uses variable steps in x with deferred correction. The codes and numerical scheme are discussed at length in Njante (2012).

We use the finite domain size $x = [-\chi/\Theta_s, 1/\Theta_s]$ for the computation. Since the slope unit $\Theta_s << 1$, we solve for $\Theta_s \to 0$; and for $\alpha \to \infty$ because then a contact angle is established. These limiting solutions complicate the analysis for the following two reasons: first, the resulting system of non-linear algebraic equations, for the coefficients of the basis functions, becomes very ill-conditioned as $\alpha \to \infty$; secondly, the problem domain becomes infinite in the limit as $\Theta_s \to 0$. This work alleviates both difficulties by using continuation in the parameters α and Θ_s. Specifically, numerical solutions are first obtained for the hydrostatic case $\alpha = 0$ and $\Theta_s > 0$ using the initial approximations; $p = 0$ and $h = 1$. The obtained solutions are then used as initial

11

225 guesses in the solution for $\alpha = \alpha + \Delta\alpha$ and $\Theta_s = \Theta_s - \Delta\Theta_s$. The process

226 is repeated until we obtain solutions for the values α and Θ_s that we desire.

227 If the value of Θ_s is not too small, then continuation in Θ_s is unnecessary.

228 For a desired value of $\Theta_s \to 0$, continuation must be used in order to avoid a

229 possible numerical singularity in the Jacobian used in the Newton iteration.

230 Figure 2 compares the numerical solution of problem (5) without approx-

231 imation with the analytic solution obtained by neglecting capillarity in the

232 differential equations (Njante 2012, equation 3.2). Within the long slowly

233 tapered section of the meniscus, capillarity is negligible. This explains the

234 good agreement between the two solutions in that part of the meniscus. The

235 agreement confirms the robustness and accuracy of our numerical scheme.

236 In the thermal model, DasGupta et el (1993) integrated the corresponding

237 equations using the shooting method. This problem differs from the thermal

238 problem because the solution continues to depend on both constants in the

239 starting series. It is for this reason that we decided to solve the problem

240 as a boundary value problem. One consequence of solving the problem as a

241 boundary value problem is that the contact angle cannot be directly obtained

242 from the model problem using a local analysis around the contact region;

243 unless the constant k described in §4 is obtained using an iterative process.

244 It is for this reason that we scale the problem, making sure that the interface

245 curvature does not vanish at the outer edge of the problem domain. Once

246 the numerical solutions are obtained on these set of scales, the contact angle

247 can then be extracted from the computed values of h as explained in §5.

12

4 Rescaling the equations

249 By its definition, the apparent contact angle $\Theta = b\Theta_s$, where the proportion-

250 ality constant b is obtained by solving problem (5). Because the solution to

251 problem (5) is a function of the parameters α, β, χ and Θ_s, so is the propor-

252 tionality constant: $b = b(\alpha, \beta, \chi, \Theta_s)$. Though problem (5) is conveniently

253 solved numerically, obtaining a correlation between b and the control param-

254 eters is non-trivial. For this work, dimensional analysis is used to obtain a

255 correlation between b and the control parameters $\alpha, \beta, \chi, \Theta_s$. The correlation

256 coefficient is obtained by comparing the result from dimensional analysis to

257 the numerical solution to problem (5). To begin, we rescale (1) by letting

$$\eta_s = \left(\frac{\nu_\ell a D_v \rho_{sat}}{R_v T_w \rho_\ell} \right)^{\frac{1}{3}}, \qquad \xi_s = \left(\frac{\gamma \rho_{sat} L \eta_s}{\rho_\ell p_{sat}(1-\phi)} \right)^{\frac{1}{3}} \qquad \text{(8a-c)}$$

258 The thickness scale η_s is the film thickness at which diffusion along the gas

259 column balances liquid flow along the film. The length ξ_s is the axial scale

260 at which Poiseuille flow driven by gradient in capillary pressure balances

261 the mass loss from the capillary. By their definition, both length scales are

262 independent of the dispersion constant A. The axial scale ξ_s is a decreasing

263 function of the potential difference $p_{sat}(1-\phi)$ driving the evaporation.

264 Table 2 shows estimates for the film thickness scale η_s and axial length

265 scale ξ_s for different channel sizes. We have used $A = 10^{-21} J$ for the dis-

266 persion constant, $L = 5a$ for the film length, and $\phi = 0.3$ for the relative

267 humidity in the distant gas. Material properties are evaluated at the uniform

268 wall temperature $T_w = 298K$. The material considered is water. As can be

269 seen from the table, the axial scale $\xi_s << a$ and the apparent contact angle,

13

270 which is proportional to the slope unit η_s/ξ_s, is about a tenth of a radian.

271   We now define new variables by

$$\eta = \frac{h_*}{\eta_s}, \qquad \xi = \frac{x_*}{\xi_s} \tag{9a,b}$$

272 Substituting these new variables into problem (1), we find that the interface

273 shape η satisfies the following boundary value problem: for $-\infty < \xi < \infty$,

$$\left[\frac{\eta^3}{3} + 1\right]\left[\frac{3\beta}{\sigma\eta^4}\frac{d\eta}{d\xi} - \frac{d^3\eta}{d\xi^3}\right] = f; \tag{10a}$$

$$as \quad \xi \to \infty: \qquad \frac{d^2\eta}{d\xi^2} \to \frac{1}{\sigma} \tag{10b}$$

$$as \quad \xi \to -\infty: \qquad \eta \to \left(\frac{\beta}{c - \sigma f\xi}\right)^{\frac{1}{3}} \tag{10c}$$

274 The domain is the real line because $\xi_s << a$ as shown in Table 2. According

275 to the mass balance equation (1a), for $h_* << \eta_s$, transport is by diffusion

276 along the gas column; boundary condition (10c) on the film thickness at

277 minus infinity is therefore obtained by neglecting both capillarity and film

278 transfer in equation (10a). The integration constant c is obtained by match-

279 ing the thin film solution (10c) to the film thickness at the channel exit. At

280 the channel exit, $\xi = -L/\xi_s$ and $\eta^3 = 1/\beta(1+\alpha)$, so that $c = \beta^2(1+\alpha) - \alpha f$.

281   The pressure ratio

$$\sigma = \left(\frac{\alpha}{\chi}\Theta_s\beta^{1/6}\right)^{2/3} \tag{11}$$

282 compares the pressure jump $\gamma\eta_s/\xi_s^2$ across the interface within the region

283 where evaporation is maximised to the pressure jump γ/a across the interface

14

at infinity. A contact angle is thus formed if $\sigma >> 1$. To verify this result, we apply the limit $\sigma \to \infty$ to equations (10) to show that η satisfies

$$\left[\frac{\eta^3}{3} + 1\right] \frac{d^3\eta}{d\xi^3} = -f; \quad \text{with} \quad \frac{d^2\eta}{d\xi^2} \to 0 \quad as \quad \xi \to \infty, \qquad \text{(12a,b)}$$

and a matching condition at $-\infty$, to be explained. According to the inner problem (10), the film thickness grows parabolically with distance as $\xi \to \infty$. This parabolic growth is necessary for matching the inner solution to the circular arc meniscus described in §2. The limit $\sigma \to \infty$ is singular for two reasons: first, disjoining pressure is negligible; an inner region Ia is therefore necessary to satisfy the thin film boundary conditions. Secondly, because the interface curvature vanishes at ∞, according to (12b), the film thickness grows linearly with distance as $\xi \to \infty$; as a result, problem (12) does not describe the parabolic arc meniscus. An outer region Ic is therefore necessary; otherwise, matching to the circular arc meniscus will be impossible. The two regions, i.e Ia and Ic, are connected together by an intermediate region Ib. We integrate the intermediate problem (12) to show that for $\xi \to \infty$,

$$\frac{d\eta}{d\xi} = k - \frac{3f}{2k^3}\xi^{-1} + o\left(1\right), \qquad p = -\frac{3f}{2k^3}\xi^{-2} + o\left(1\right) \qquad \text{(13a,b)}$$

where k is an integration constant. Equation (13b) shows that the the vapour pressure asymptotically approaches the saturation pressure at the outer edge of the intermediate region; as a result, the vapour pressure is asymptotically equal to the saturation pressure throughout the entire region described by the parabolic are meniscus; evaporation from the parabolic arc meniscus is therefore asymptotically negligible. All the evaporation thus occurs within

15

sub-regions Ia and Ib. However, as concluded by Njante(2012, equation 3.4), for $\alpha \to \infty$, evaporation from the precursor film is negligible; as a result, the intermediate region Ib determines the total evaporation from the capillary.

Equation (13a) shows that the apparent contact angle is well defined. The correction term of $O\left(\xi^{-1}\right)$ is included to stress that the slope approaches a limit at infinity. The stationary evaporating meniscus thus differs from the moving isothermal meniscus. The dynamic contact angle in that problem is poorly-defined: though the curvature vanishes at infinity, the slope there continues to grow as $(\ln \xi)^{1/3}$ (see de Gennes 1985, Equation 4.29). The slope thus depends weakly on position x whereas in the present case, it approaches a limit at infinity. Because the slope approaches a limit at the outer edge of the intermediate region, an apparent contact angle Θ is established there. Specifically, $\Theta = (\eta_s/\xi_s)k$. Comparing with $\Theta = b\Theta_s$, we find that

$$ b = k\beta^{1/6}\sqrt{\sigma} \qquad \text{where} \qquad k = \lim_{\sigma \to \infty} \lim_{\eta \to \infty} \left(\frac{d\eta}{d\xi} \right). \qquad (14\text{a,b}) $$

We have used equations (3a,6) to express $\eta_s/\xi_s\Theta_s$ as a function of the control parameters. By (14b), a contact angle is established for $\sigma \to \infty$. However, because $\Theta \sim \eta_s/\xi_s$, the expression for Θ does not contain a/ξ_s. Consequently, the contact angle Θ can be of order unity, even though $\sigma = a\eta_s/\xi_s^2 >> 1$.

5   Obtaining b numerically

According to boundary condition (1f), the interface curvature approaches a constant at the outer edge of region I; the film thickness thus grows parabolically with distance as $x \to \infty$. If the parabola so defined has a zero, then a

16

contact angle is defined by the slope at $h = 0$. Since the entire interface does not have a constant curvature, an apparent contact angle is defined by first computing the constant curvature profile for large h, and then extrapolate down to $h = 0$. To give a precise definition of Θ using this method, we multiply the asymptotic relation $d^2h/dx^2 \sim 1$ by $2dh/dx$, and then integrate once in x to show that $(dh/dx)^2 \sim 2h + b^2$, where b^2 is the integration constant. We therefore use the definition $\Theta = b\Theta_s$, where the integration constant

$$b^2 = \lim_{\sigma \to \infty} \lim_{h \to \infty} \left[\left(\frac{dh}{dx} \right)^2 - 2h \right] \tag{15}$$

According to boundary value problem (5), for $\alpha = 0$, the system is in hydrostatic equilibrium; for $\alpha > 0$, the liquid pressure at the channel exit is less than the bulk liquid pressure. As a result, liquid flows from the bulk meniscus into the contact region; σ is proportional to the pressure gradient driving that flow. The limit $\sigma \to \infty$ in equation (15) therefore ensures that the liquid motion is strong enough to distort the liquid-gas interface and also to create an apparent contact angle Θ. The other limit $h \to \infty$ picks out the constant curvature part of the phase interface, and also ensures that the apparent contact angle defined by equation (15) is independent of film thickness. Numerical solutions are now used to establish the existence of Θ.

Figure 3 shows the interface curvature d^2h/dx^2 computed without approximation from the inner problem (5) as a function of film thickness h; on the right hand side of the figure, $d^2h/dx^2 \to 1$, as required by boundary condition (5f). Near the origin, however, $d^2h/dx^2 \to 1$ has a local maximum for 3 of the 4 curves. The maximum value is an increasing function of the potential difference $p_{sat}(1 - \phi)$ driving evaporation. For $\phi = 1$, the system is

17

in hydrostatic equilibrium; for $\phi < 1$, the partial pressure at the channel exit is less than the value required for the liquid to coexist in equilibrium with its vapour, and as a result, liquid evaporates from the extended meniscus. This explains why the interface shape is not perturbed for $\sigma \to 0$, bottom curve. For $\sigma \to \infty$ however, the flow becomes strong enough to perturb the interface, and as a result, creates an apparent contact angle, see the top three curves. Figure 3 therefore supports the limit define in equation (15).

Figure 4 shows the squared interface slope $(dh/dx)^2$ computed from the inner problem (5) without approximation as a function of film thickness h; as expected, $(dh/dx)^2$ is an increasing function of the potential difference driving evaporation. On the right hand side of the figure, $(dh/dx)^2$ grows linearly with h; this linear growth marks the constant curvature portion of the phase interface. The limit $h \to \infty$ in equation (15) thus picks out the constant curvature part of the phase interface as claimed earlier. As can be seen from the graphs, the interface curvature becomes uniform only for film thicknesses $h > 10$. Therefore to extract b from the computed values of h, we first discard all data for $h < 10$, and then fits a straight line to the rest using the least square method. The intercept of that line determines b^2.

6   Computation of k

Computing k directly from (10) requires significant computing power. For this reason, we find k by comparing the scaling relation (14) to the numerical solution for b obtained in the previous section. To begin, we note that because the solution to (10) depends on σ and β, so is the integration constant k.

18

371 Consequently, for $\sigma \rightarrow \infty$, the constant k is a function of β alone. Therefore

372 keeping β fixed, equation (14) predicts that a plot of b against $\beta^{1/6}\sqrt{\sigma}$ should

373 give a straight line, whose slope k depends on the size of β alone.

374 Figure 5 shows the integration constant b computed from (5) using the

375 method described in §5 as a function of $\beta^{1/6}\sqrt{\sigma}$. As expected, b is a linear

376 function of $\beta^{1/6}\sqrt{\sigma}$; the slope k of each line is a function of β. The very

377 small scatter in the numerical solutions is a clear indication that k is a very

378 weak function of β. Armed with this information, we plot b as a function of

379 the parameter $\beta^{\delta}\beta^{1/6}\sqrt{\sigma}$, where the exponent $\delta << 1$ is chosen, by trial and

380 error, so as to collapse the numerical solutions onto a single straight line.

381 Figure 6 shows that the choice $\delta = 4/225$ collapses the numerical solutions

382 onto a single straight line as $\beta^{\delta}\beta^{1/6}\sqrt{\sigma} \rightarrow \infty$; this implies that the slope

383 parameter $b \rightarrow s\beta^{\delta}\beta^{1/6}\sqrt{\sigma}$ as $\beta^{\delta}\beta^{1/6}\sqrt{\sigma} \rightarrow \infty$, where s is the slope of the line.

384 The figure shows that the numerical solutions collapse onto the straight line

385 only for values of $\beta^{\delta}\beta^{1/6}\sqrt{\sigma} > 3$. Therefore, to obtain s from the numerical

386 solutions, we first discard all data for $\beta^{\delta}\beta^{1/6}\sqrt{\sigma} < 3$, and then fits a line to

387 the rest using the least square method. The slope of that line determines s.

388 Using this method, we find that $s \simeq 1.76$. The related expression for b is

$$b = 1.76\beta^{4/225}\beta^{1/6}\sqrt{\sigma} \qquad as \qquad \sigma \rightarrow \infty \qquad (16)$$

389 Equation (16) provides a useful correlation between b, σ, and β. Comparing

390 this result to the scaling relation (14), we find that $k = 1.76\beta^{4/225}$, which

391 is a very weak function of β as suggested in figure 5. The corresponding

392 expression for the apparent contact angle, $\Theta = (\eta_s/\xi_s)k$, is given by

19

$$\Theta = kCa^{1/3} \qquad where \qquad Ca = \frac{\nu_\ell \dot{m}_s}{\gamma \eta_s} \qquad (17\text{a,b})$$

We have used equation (8) for η_s/ξ_s and the definition $Ca = \mu_\ell V_s/\gamma$ for a capillary number based on a velocity scale $V_s = \dot{m}_s/\rho_\ell \eta_s$ set by evaporation. By its definition, Ca is independent on the dispersion constant A; and as a result, micro-physics affects Θ only through the integration constant k. We recall that $k = 1.76\beta^{4/225}$ is a function of the dispersion constant through β.

Figure 7 shows k as a function of β. The graph shows that the contact angle depends very weakly on micro-physics, except for $\beta \to 0$. Physically, the film thickness at which the contact angle is established is proportional to the parameter $\beta^{1/3}$. Therefore for $\beta \to 0$, the contact angle is established at the scale where disjoining pressure is significant. This also explains why the contact angle varies weakly with β for large β; here, Θ is established at a scale where disjoining pressure is insignificant. These effects can also be explained by first noting that β measures the viscous resistance to liquid flow; which implies that for large β, liquid motion, and hence the distortion of the interface, occurs at a much larger scale than that at which disjoining pressure is significant. Figure 7 covers a sufficiently wide range of β, including the range typical in applications. Specifically, it covers $10^{-3} \le \beta \le 10^3$, and the figure shows that over this range of β, the integration constant

$$1.5 < k < 2.0 \qquad so \ that \qquad \Theta = 1.75Ca^{1/3} \qquad (18\text{a,b})$$

with very little error. Equation (18b) expresses the apparent contact angle as a function of a single parameter Ca depending only on well-known macro-

20

physical properties. Though micro-physics must be included in the boundary value problem in order to resolve a hydrodynamic singularity at the contact line, Θ is insensitive to the microphysical details. The insensitivity of Θ to the value of the dispersion constant has been obtained before for the thermal problem by Stephan and Busse (1992) and by Morris (2001). In agreement with the heuristic argument of Poulard et al (2005, Equation 14), Θ varies as the one-third power of a capillary number based on the evaporation rate.

Unlike the thermal problem, the apparent contact angle for a diffusion controlled evaporating meniscus is a function of the capillary size. To explain why, we first note that the contact angle increases with the evaporation rate, irrespective of the boundary condition driving the evaporation. In the case of a diffusion-controlled evaporating system however, the rate of evaporation is proportional to the capillary radius. This explains why the contact angle here increases with the outer length scale. In the thermal problem, the outer length scale enters the problem only through an outer boundary condition describing the bulk meniscus. Because a local analysis around the contact region does not include that outer boundary condition, the apparent contact angle for the thermal problem is independent on the outer length scale.

7 Conclusion

To analyse the evaporating meniscus, we have used the separation of scales described in §2. The inner region consists of a quasi–parallel liquid film, and the corresponding portion of the gas column. Within this region, the lubrication approximation holds within the film and, across the gas column, the

partial pressure of the vapour is uniform. Owing to these two conditions, the unknowns depend only on distance along the wall, and the mass transport within the inner region is determined by boundary value problem (1) containing only ordinary differential equations. For the gas, the outer region is bounded by the visible circular arc meniscus, above which the vapour partial pressure p_v^* is asymptotically equal to the saturation pressure throughout the entire region. The first conclusion of this work is that the liquid and vapour flow is completely determined by the solution of the inner problem (1).

Poulard et al (2005) have shown experimentally that the diffusion controlled meniscus of a perfectly wetting system exhibits an apparent contact angle; Θ vanishes when the system is in hydrostatic equilibrium, and is an increasing function of the potential difference $(1 - \phi)p_{sat}$ driving evaporation. For the first time, we have posed and solved a boundary value problem whose solution exhibits an apparent contact angle. We give the condition under which the apparent contact angle will be observed; as Figure 3, we give numerical results demonstrating this condition. As equation (16), we give a scaling law describing the dependence of Θ on the control parameters in the theory. Lastly, as equation (18b) we give an explicit formula for Θ as a function of a capillary number Ca, depending only on well-known macro-physical properties; even though microphysics must be included in the boundary value problem in order to resolve a hydrodynamic singularity at the contact line, the apparent contact angle Θ is insensitive to the microphysical details.

22

A Derivation of the Governing Equations

A.1 Conditions Under Which The Simplified Kinetic Equation (1c) Holds

Let $\mathcal{P}(T, p_\ell^*)$ be the local co-existence pressure; i.e the vapor pressure required for liquid and vapor to co-exist at temperature T and pressure p_ℓ^*. Then by kinetic theory, $CJ^*/\lambda = (\mathcal{P} - p_v^*)$, see Cammenga (1980). Liquid thus evaporates at any point along the interface if the vapor pressure on the gas side of the interface is less than the co-existence pressure. Also, let p_o be the vapor pressure at the exit of the channel, and T_o the temperature at which liquid and vapor co-exist when both are at pressure p_o. Then following Morris (2000), the kinetic equation is simplified by expanding $(\mathcal{P} - p_v^*)$ in a Taylor series about the reference state (p_o, T_o). To a first order approximation,

$$\frac{CJ^*}{\lambda} = \frac{\rho_s Q}{T_o}(T - T_o) + \frac{\rho_s}{\rho_\ell}(p_\ell^* - p_o) - (p_v^* - p_o) \tag{19}$$

where ρ_ℓ is the liquid density, Q the latent heat of vaporization, C the speed of sound in the gas, $\lambda = \sqrt{2\sigma/\pi}$ a kinetic constant, σ the specific heat ratio, and ρ_s the saturation vapour density at temperature T_o. In the thicker portions of the meniscus, i.e on the scale of the channel gap thickness, diffusion is rate limiting; as a result, the term on the left of (19) vanishes far from the contact line. Hence, we apply the condition that $J \to 0$ at infinity to obtain

$$0 = \frac{\rho_s Q}{T_o}(T_w - T_o) + \frac{\rho_s}{\rho_\ell}(p_b - p_o) - (p_s - p_o) \tag{20}$$

23

where far from the wall, the interface temperature is assumed to be equal to the wall temperature; evaporative cooling is therefore taken as negligible at infinity. p_s is the saturation pressure at temperature T_o. Equation 20 gives T_o as a function of the boundary values p_b, p_s, p_o, and T_w which are all given as part of the solution. By subtracting equation 20 from 19, we obtain

$$\frac{CJ^*}{\lambda} = \frac{\rho_s Q}{T_o} (T - T_w) + \frac{\rho_s}{\rho_\ell} (p_\ell^* - p_b) - (p_v^* - p_s) \tag{21}$$

In equation 21, T_o can be replaced by T_w because $|T_w - T_o| << T_o$ in applications. We have therefore eliminate T_o and p_o in favour of known boundary values. Because there is no build up of mass at the interface, specie mass balance there requires that the rate of transfer of molecules across the interface be equal to the diffusion flux evaluated at the interface. Specifically

$$-\Lambda \frac{\partial p_v^*}{\partial n} = \frac{\rho_s Q}{T_w} (T - T_w) + \frac{\rho_s}{\rho_\ell} (p_\ell^* - p_b) - (p_v^* - p_s) \tag{22}$$

where $\Lambda = CD_v/\lambda R_v T_w$ is the mean free path of the vapor molecules in the gas. The mixed boundary condition (22) couples the dynamical processes in the surrounding gas to those in the liquid phase. This coupling of the different physics make direct analysis difficult. We therefore make the following simplifying assumptions: (i) The continuum approximation holds within the surrounding gas; as a result, liquid and vapor at the interface are in local thermodynamic equilibrium. (ii) The system is effectively isothermal; though evaporation induces liquid temperature differences, they are kinetically negligible for the slow evaporation processes considered here.

Given (i) and (ii), equation 22 simplifies to

24

$$p_v^* = p_s + \frac{\rho_s}{\rho}(p_\ell^* - p_b) \qquad (23)$$

A.2   Conditions for Isothermal Evaporation

The latent heat consumption caused by evaporation at the interface induces temperature gradients within the drop, substrate, and surrounding gas. One can estimate the order of magnitude for temperature differences within the drop by making use of the energy balance $\kappa \nabla T \cdot n_1 = Q J^*$ at the interface, where κ is the liquid thermal conductivity, n_1 the unit normal to the interface with the other parameters defined above. The energy balance states that all heat conducted from the wall to the interface is absorbed as latent heat. Because there is no build up of mass at the interface, the evaporative flux term J is estimated using Fick's law $J = D_v \nabla c \cdot n_2$, where n_2 is the unit normal at the interface into the gas and $c = p_v^*/R_v T_w$. Eliminating J between the two equations, Fick's law and energy balance, we find that at the interface

$$\kappa \frac{\partial T}{\partial n_1} = \frac{Q D_v}{R_v T_w} \frac{\partial p_v^*}{\partial n_2} \qquad (24)$$

To a first approximation, the vapour flow occurs in a half-space and so has just one length scale δ/Θ, where δ is a characteristic film thickness. Near the contact line, where temperature differences across the drop are highest, the liquid flow occurs in a wedge of contact angle Θ, and so has two length scales δ/Θ and δ. Then, according to equation 24, we estimate that

25

$$\Delta T \sim \Theta \frac{QD_v}{\kappa R_v T_w} p_s (1 - \phi) \tag{25}$$

where p_s is the saturation vapour pressure, ϕ the relative humidity in the distant gas, and ΔT the characteristic temperature difference across the drop. According to equation 22, temperature differences within the drop are kinetically negligible if the first term on the right is negligibly small as compared to the third term; i.e if $\rho_s Q \Delta T / T_w << p_s(1 - \phi)$, which translates to

$$\epsilon = \frac{\rho_s Q^2 D_v \Theta}{\kappa R_v T_w^2} << 1 \tag{26}$$

Both ϵ and ΔT depend on the drop size through Θ. The parameter ϵ is given in Sultan et al (2005, row 7, table 2) as the ratio of a thermal expansion number to a kinetic Peclet number; in their notation $\epsilon = \chi / Pe_k$.

In table 3, we give some estimates for the parameters. Values of Θ for the first two rows are taken from Cachile et al (2002); the last row from Deegan et al (2000). The relative humidity $\phi = 0$ for the organic liquids and $\phi = 0.4$ for water. The table shows that temperature gradients, and hence Marangoni flows, become increasingly significant as the drop thickness increases; i.e for drops with large Θ. This does not mean that heat conduction becomes the controlling mechanism because for that to happen, the drop size must be small compared with the mean free path Λ of the vapour in the gas.

A.3 Derivation of Equation (1a)

To simplify the problem, we assume that transport of the vapour molecules in the gas is by axial diffusion only; though there are concentration gradients in

26

the radial direction, they are negligibly small in the limit $a/L \to 0$. Balancing

mass on the differential control volume in figure **??**a requires that

$$\dot{m}_x + \dot{m}_g - \dot{m}_{x+dx} = \frac{d}{dt} m_{sys} \tag{27}$$

Where $\dot{m}_x$ is the rate at which mass is entering the control volume, $\dot{m}_g$ the

rate at which mass is generated within the control volume, $\dot{m}_{x+dx}$ the rate

at which mass is leaving the control volume, and m_{sys} the total mass within

the control volume at any given instant. These quantities are given as

$$\dot{m}_x = \frac{D_v p}{R_v T_w} A_c(x) \frac{d}{dx} \ln\left(1 - \frac{p_v}{p}\right) \tag{28a}$$

$$\dot{m}_g = J(x) dA_s \tag{28b}$$

$$\dot{m}_{x+dx} = \dot{m}_x + \frac{d\dot{m}_x}{dx} dx \tag{28c}$$

Where $A_c(x)$ is the cross-sectional area of the channel, dA_s the surface area

of the differential element, $p_v(x)$ the vapour pressure, $J(x)$ the evaporative

mass flux normal to the interface, p the total gas pressure, D_v the binary

diffusion coefficient, R_v the specific gas constant, and T_w the wall tempera-

ture. Equation 28a expresses Fick's first law; it assumes that the medium

into which evaporation occurs is stationary, and that the gas mixture is ideal.

Taylor expanding equation 28a gives us 28c. For a channel made up of two

parallel plates, $A_c(x) = a - h(x)$ and $dA_s = dx$ per unit depth of channel.

Due to symmetry, we have considered only the lower half of the channel.

Under steady state conditions, equations 27 and 28 gives

$$J = \frac{D_v p}{R_v T_w} \frac{d}{dx} \left[(a - h) \frac{d}{dx} \ln \left(1 - \frac{p_v}{p} \right) \right] \tag{29}$$

Using lubrication theory, the mass flow rate in the thin quasi-parallel liquid film is related to the local evaporative mass flux J by

$$\frac{d}{dx} \left[\frac{h^3}{3\nu} \frac{dp_\ell}{dx} \right] = J \tag{30}$$

Equation (30) neglects shear stress at the interface. We now eliminate J between equations (29) and (30); then integrate once to show that

$$\frac{h^3}{3\nu} \frac{dp_\ell}{dx} - \frac{D_v p}{R_v T_w} (a - h) \frac{d}{dx} \ln \left(1 - \frac{p_v}{p} \right) = -\dot{m} \tag{31}$$

For $p_v/p \to 0$ and for $h << a$, equation (31) reduces to (1a).

28

Liquid	$10^{-4}\alpha$	β	Θ_s
Heptane	0.5529	0.2072	0.0282
Octane	0.4550	0.3107	0.0277
Water	1.3280	0.2113	0.0228

Table 1: Estimates of parameters

$a(\mu m)$	$\eta_s(nm)$	$\xi_s(nm)$	η_s/ξ_s	$10^{-3}a/\xi_s$
10	12	76	0.154	0.13
1000	55	590	0.093	1.69

Table 2: Characteristic dimensions of the contact region

Liquid	$\Theta(rad)$	$\Delta T(K)$	ϵ
Octane[2]	0.015	0.10	0.007
Heptane[2]	0.030	0.23	0.011
Water[5]	0.26	15.62	1.56

Table 3: Estimates for ΔT and ϵ
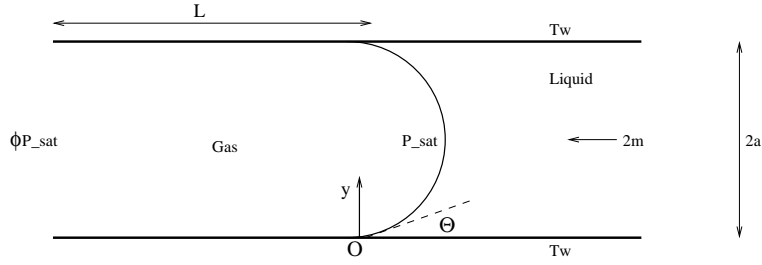
Figure 1: The evaporating meniscus in a channel as seen on the scale of the channel gap thickness $2a$. The origin is at point O, with the positive x-axis to the right.
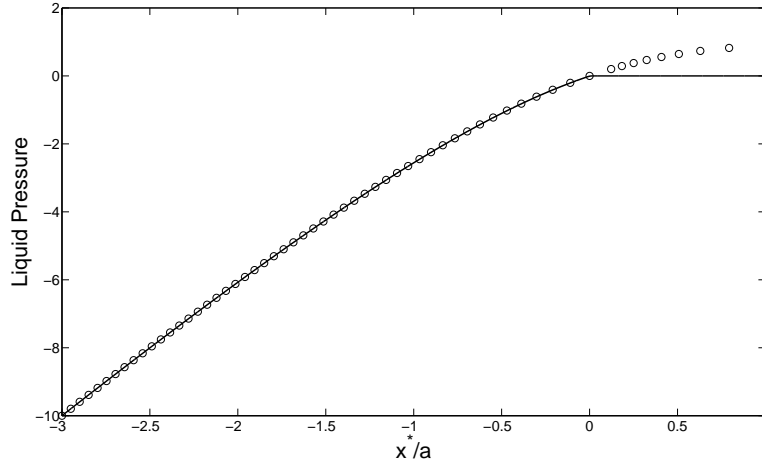
Figure 2: Liquid pressure $(p_\ell^* - p_b)a/\gamma$ as a function of position x^*/a: open circles, analytic solution obtained from problem (5) by neglecting the first term on the right of equation (5b); solid curve, computed without approximation from (5). With $\chi = 3$, $\alpha = 10$, $\beta = 0.2$, and $\Theta_s = 0.01$: for χ, α, β, and Θ_s, see (6) and (3) respectively.
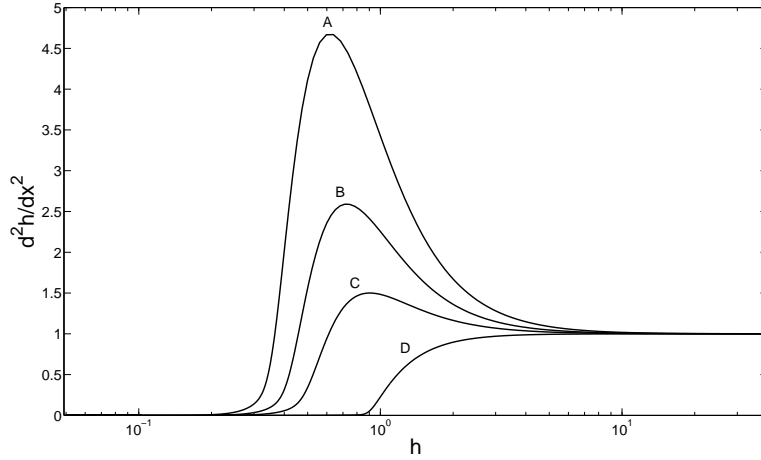
Figure 3: Interface curvature $a(d^2h^*/dx^{*2})$ computed without approximation from the inner problem (5) as a function of film thickness $h = h^*/h_s$. The curves represent values computed for: A, $\sigma = 10$; B, $\sigma = 6$; C, $\sigma = 4$; D, $\sigma = 0.5$. The length scale h_s is defined in equation (3) while the parameters β and σ are defined in equations (6,11).
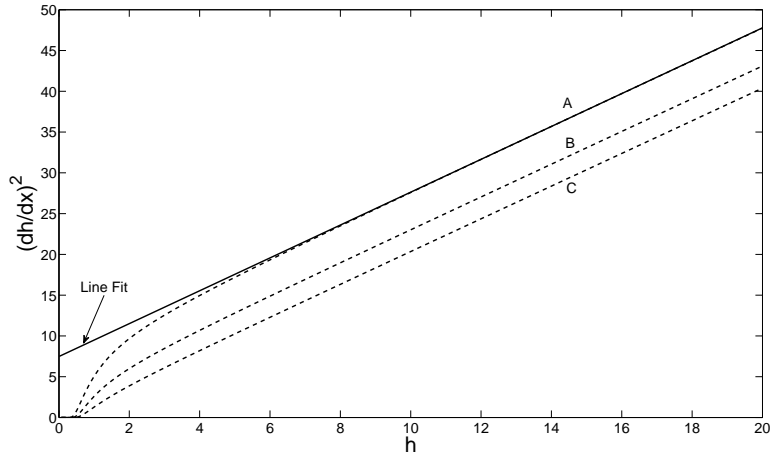

Figure 4: Squared interface slope $(\gamma a^2/A)^{1/3}(dh^*/dx^*)^2$ computed without approximation from the inner problem (5) as a function of film thickness $(\gamma/aA)^{1/3}h^*$. Broken curves represent values computed for: A, $\sigma = 10$; B, $\sigma = 6$; C, $\sigma = 4$. These are the same values used in computing figure 3. The solid line represents a line fit for large h, using the least square method. See definitions (11,6) for the parameters σ and β respectively.
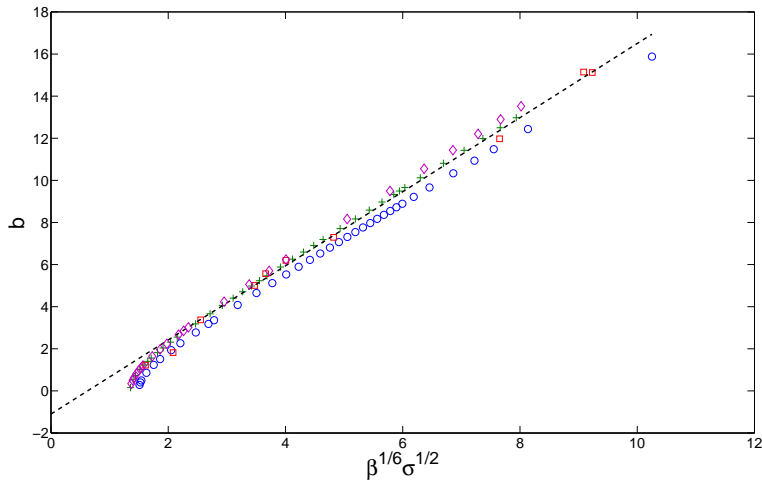
31

Figure 5: Slope parameter b as a function of the parameter $\beta^{1/6}\sqrt{\sigma}$: Symbols denote values computed without approximation from problem (5) using the definition (15) of b: Triangles, $\beta = 10$; open circles, $\beta = 0.1$; plus sign, $\beta = 1$; and squares for selected values of β between 0.01 and 30. These values include the range typical in applications.
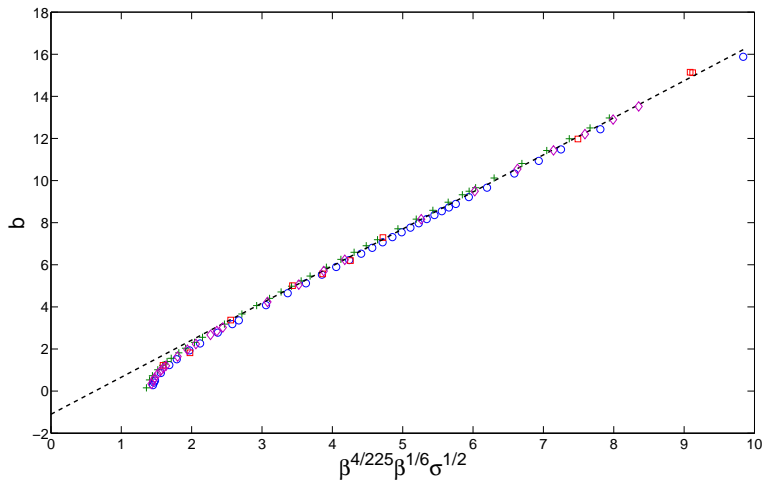

Figure 6: Slope parameter b as a function of the parameter $\beta^{4/225}\beta^{1/6}\sqrt{\sigma}$: Symbols denote values computed without approximation from problem (5) using the definition (15) of b: Triangles, $\beta = 10$; open circles, $\beta = 0.1$; plus sign, $\beta = 1$; and squares for selected values of β between 0.01 and 30. These values include the range typical in applications.

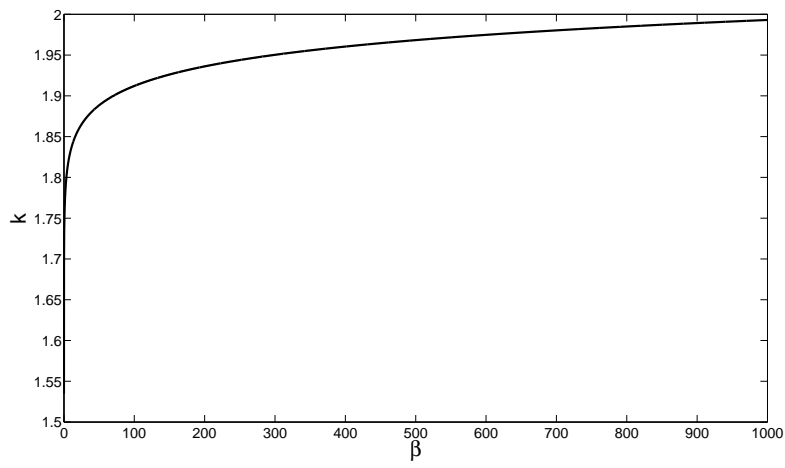Figure 7: Effects of micro-physics on Θ.

REFERENCES

1. BIRD, R. B., STEWART, E. W., & LIGHTFOOT, N. E. 2006 Transport Phenomena. Wiley, New York.

2. CACHILE, M., BENICHOU, O., & CAZABAT, A-M, 2002 Evaporating Droplets of Completely Wetting Liquids. Langmuir **18**, 7985-7990

3. CAMMENGA, H. K. 1980 Evaporation mechanisms of liquids. Current topics in materials science **5**.

4. DASGUPTA, S., SCHONBERG, J. A., KIM, I. Y., & WAYNER, P. C. 1993 Use of the Augmented Young-Laplace Equation to Model Equilibrium and Evaporating Extended Meniscus. J. Colloid Int. Sci. **157**, 332-342.

5. DEEGAN, R. D., BAKAJIN, O., DUPONT, T. F., HUBER, G., NAGEL, S. R., and WITTEN, T. A. 2000 Contact Line Deposits in an Evaporating Drop. Phys. Rev. E **62**, 756-765, No 1.

6. DE GENNES, P. G. 1985 Wetting: statics and dynamics. Rev. Mod. Phys. **57**, No. 3, Part 1, 93-98.

7. DERJAGUIN, B. V., NERPIN, S. V., & CHURAYEV, N. V. 1965 Effect of film transfer upon evaporation of liquids from capillaries. Bulletin Rilem **29**, 93-98.

8. LEVINSON, P., VALIGNAT, M.P., FRAYSSE, N., CAZABAT, A.M., & HESLOT, F. 1993 An ellipsometric study of adsorption isotherms. Thin Solid Films **234**, 482-485

34

9. MORRIS, S.J.S. 2001 Contact angles for evaporating liquids predicted and compared with existing experiments. J. Fluid Mech. **432**, 1-30.

10. NJANTE, J-P. 2012 Diffusion-Controlled Evaporating Completely Wetting Meniscus in a Channel. Ph.D Thesis, UC Berkeley.

11. POULARD, C., GUENA, G., CAZABAT, A-M, BOUDAOUD, A., & AMER, B.M. 2005 Rescaling the Dynamics of Evaporating Drops. Langmuir **21**, pp. 8226-8233

12. RENK, F., WAYNER, P. C., & HOMSY, G. M. 1978 On the transition Between a Wetting Film and a Capillary Meniscus. J. Colloid Int. Sci. **67**, No 3, 408-414

13. STEPHAN, P. C. & BUSSE, C. A. 1992 Analysis of the heat transfer coefficient of grooved heat pipe evaporator walls. Int. J. Heat Mass Transfer **35**, No2, 383-391.

14. SULTAN, E., BOUDAOUD, A., & AMER, M. B. 2005 Evaporation of a thin film: diffusion of the vapour and marangoni instabilities. J. Fluid Mech. **543**, 183-202.

15. TRUONG, J. G. & WAYNER, P. C. 1987 Effect of Capillary and Van der Waals Dispersion Forces on the Equilibrium Profile of a Wetting Liquid: Theory and Experiment. J. Chem. Phys. **87**, 4180-4188